#### **PROCEEDINGS A**

royalsocietypublishing.org/journal/rspa

### Research



**Cite this article:** Tien M-H, D'Souza K. 2020 Method for controlling vibration by exploiting piecewise-linear nonlinearity in energy harvesters. *Proc. R. Soc. A* **476**: 20190491. http://dx.doi.org/10.1098/rspa.2019.0491

Received: 1 August 2019 Accepted: 22 November 2019

#### **Subject Areas:**

energy, mechanical engineering, power and energy systems

#### **Keywords:**

energy harvesting, vibration control, bilinear, piecewise-linear, nonlinear, adaptive tracking

#### **Author for correspondence:**

Kiran D'Souza

e-mail: dsouza.60@osu.edu

Electronic supplementary material is available online at https://doi.org/10.6084/m9. figshare.c.4794546.

# Method for controlling vibration by exploiting piecewise-linear nonlinearity in energy harvesters

Meng-Hsuan Tien and Kiran D'Souza

Department of Mechanical and Aerospace Engineering, The Ohio State University, 2300 West Case Road, Columbus, OH 43235, USA

M-HT, 0000-0002-1844-0093

Vibration energy is becoming a significant alternative solution for energy generation. Recently, a great deal of research has been conducted on how to harvest energy from vibration sources ranging from ocean waves to human motion to microsystems. In this paper, a theoretical model of a piecewise-linear (PWL) nonlinear vibration harvester that has potential applications in variety of fields is proposed and numerically investigated. This new technique enables automatic frequency tunability in the energy harvester by controlling the gap size in the PWL oscillator so that it is able to adapt to changes in excitations. To optimize the performance of the proposed system, a control method combining the response prediction, signal measurement and gap adjustment mechanism is proposed in this paper. This new energy harvester not only overcomes the limitation of traditional linear energy harvesters that can only provide the maximum power generation efficiency over a narrow frequency range but also improves the performance of current nonlinear energy harvesters that are not as efficient as linear energy harvesters at resonance. The proposed system is demonstrated in several case studies to illustrate its effectiveness for a number of different excitations.

# 1. Introduction

Vibration energy harvesting is considered one of the most promising green energy sources that can self-power small-scale devices and fulfill the need of large-scale electricity generation. On the one hand, as electronic devices are becoming more compact and portable, a

sustainable and scalable energy source with high-energy density is in high demand [1,2]. Ambient vibration is an ideal energy source for these systems since it is ubiquitous and easily accessible. On the other hand, large-scale vibrations such as those from ocean waves are now considered to be a potential energy resource to power entire cities since they contain great source of recoverable energy [3,4]. Thus, vibration energy harvesting is an attractive solution in fulfilling a variety of energy needs and a significant amount of research has been conducted to optimize energy extraction from vibration sources [5].

Vibration energy harvesting can be realized using piezoelectric [6-8], electromagnetic [9-11] or electrostatic [12] approaches. Early designs of these power generators were based on linear models [13-17] that provide the maximum power generation efficiency at resonance with their efficiency decreasing dramatically even when the excitation frequency shifts slightly. Thus, traditional linear energy harvesters are usually limited to very narrow frequency ranges. In order to broaden the frequency bandwidth for effective energy harvesting, different techniques such as nonlinear energy harvesting [2,18-27], array-harvester systems [28,29], and frequencytunable systems [30] have been developed so the harvester can accommodate a broader frequency range. Each technique has its own advantages and disadvantages. For instance, the array-harvester design can harvest the vibration energy over resonant frequencies of each linear system; however, the system set-up and the corresponding electronic configuration are complex, which makes the utilization very challenging [5]. Nonlinear energy harvesters [2,18-27], which are commonly used in piezoelectric and electromagnetic generators, can broaden the effective frequency bandwidth by exploiting geometric and material nonlinearities; however, these nonlinear techniques are not as efficient as linear energy harvesters at resonance.

Recently, new designs of energy harvesters with piecewise-linear (PWL) nonlinearities have been proposed [31–39]. These nonlinear devices incorporate mechanical stoppers into conventional linear energy harvesters. It is found that these PWL harvesters can effectively broaden the effective frequency range for an up-sweep excitation condition. However, these devices do not guarantee the best vibration performance at an arbitrary excitation frequency. Also, they do not achieve the efficiency of linear harvesters at resonance.

In this paper, a theoretical model of a new vibration harvester composed of a PWL oscillator and a controllable gap is proposed and investigated. In this new design, the resonant frequency of the harvester can be tuned to match the dominant frequency of the excitation to provide the instantaneous optimized vibration performance. The frequency tunability is enabled by adjusting the gap size in the PWL oscillator. Furthermore, a control method combining the response prediction, signal measurement, and gap adjustment mechanism is proposed to optimize the system's performance. In this control method, a response approximation technique referred to as the bilinear amplitude approximation (BAA) method [40] is first used to compute the gap size that can tune the system to resonance over an effective frequency range. BAA is one of the techniques developed recently to efficiently capture the nonlinear response of PWL nonlinear systems using linear techniques [40-42]. Frequency and amplitude estimators are then employed to analyse the excitation signal over a specified time window. The gap in the PWL oscillator is then adjusted to the appropriate size that can optimize the vibration performance based on the measured excitation signal and the pre-computed optimized gap size. The proposed energy harvesting strategy has a better performance than current PWL harvesters since it provides a better vibration performance for both stationary excitation and drifting excitation conditions.

The remainder of the paper is organized as follows. In §2, the system configuration and its mechanical model are introduced. In §3, the dynamic properties of the proposed system is investigated and discussed. In §4, the control method proposed to optimize the vibration performance of the device is presented. In §5, the vibration performance of the proposed system and method are numerically investigated and compared with current techniques. In §6, the coupling of the mechanical model and energy transducer, and future research directions are discussed. Finally, conclusions are given in §7.

## 2. System configuration and modelling

The system configuration of the proposed PWL harvester and its mechanical model are shown in figure 1 and introduced in this section. The proposed system is composed of a mass m, a linear spring with stiffness k attached to the mass, and another linear spring with stiffness  $k^*$  that has intermittent contact with the mass. The system is assumed to be damped with damping coefficient c and  $c^*$ . The gap size g(t) between the mass m and the linear spring  $k^*$  is adjustable through a linear actuator or a positioning system attached to the frame of the device. Note that the time variation of the gap size is caused by the change of the reference point controlled by the linear positioning system not by the displacement of the mass. The harvester is assumed to be subjected to a base excitation with base displacement y(t). The displacement of the mass m is denoted using x(t). The equations of motion of the system can be expressed as

$$m\ddot{x}_{c}(t) + (c + c^{*})\dot{x}_{c}(t) + (k + k^{*})\bar{x}_{c}(t) = -m\ddot{y}(t) + c^{*}\dot{g}(t) + k^{*}g(t) \quad \text{when } \bar{x} \ge g,$$

$$m\ddot{x}_{o}(t) + c\dot{x}_{o}(t) + k\bar{x}_{o}(t) = -m\ddot{y}(t) \quad \text{when } \bar{x} < g,$$
(2.1)

where  $\overline{x} = x - y$  represents the relative displacement between the mass m and the moving base. Note that the subscript c represents the displacement of the mass when the gap is closed, i.e.  $\overline{x} \ge g$ , and the subscript o represents the displacement of the mass when the gap is open, i.e.  $\overline{x} < g$ . Equation (2.1) can then be rewritten as

$$\frac{\ddot{x}_{c}(t) + 2(\zeta\omega + \zeta^{*}\omega^{*})\dot{x}_{c}(t) + (\omega^{2} + \omega^{*2})\overline{x}_{c}(t)}{= -\ddot{y}(t) + 2\zeta^{*}\omega^{*}\dot{g}(t) + \omega^{*2}g(t)} \qquad \text{when } \overline{x} \ge g, 
\frac{\ddot{x}_{o}(t) + 2\zeta\omega\dot{x}_{o}(t) + \omega^{2}\overline{x}_{o}(t) = -\ddot{y}(t)}{= -\ddot{y}(t)} \qquad \text{when } \overline{x} < g,$$
(2.2)

and

and

where  $\omega^2 = k/m$ ,  $\omega^{*2} = k^*/m$ ,  $\zeta = c/2m\omega$ , and  $\zeta^* = c^*/2m\omega^*$ . In this paper, it is assumed that the system is driven by a harmonic excitation  $y(t) = y_0 \sin(\alpha t)$ , where  $y_0$  is the excitation amplitude and  $\alpha$  is the excitation frequency.

Next, dimensionless variables [36] are introduced to simplify the subsequent analysis. First, the time-related dimensionless variables are introduced

$$\tau = \omega t, \quad \rho = \frac{\alpha}{\omega} \quad \text{and} \quad \rho^* = \frac{\omega^*}{\omega}.$$
 (2.3)

Equation (2.2) can then be expressed as

$$\overline{x}_{c}''(\tau) + 2(\zeta + \zeta^{*}\rho^{*})\overline{x}_{c}'(\tau) + (1 + \rho^{*2})\overline{x}_{c}(\tau)$$

$$= \rho^{2}y_{0}\sin(\rho\tau) + 2\zeta^{*}\rho^{*}g'(\tau) + \rho^{*2}g(\tau) \qquad \text{when } \overline{x} \ge g,$$

$$\overline{x}_{o}''(\tau) + 2\zeta\overline{x}_{o}'(\tau) + \overline{x}_{o}(\tau) = \rho^{2}y_{0}\sin(\rho\tau) \qquad \text{when } \overline{x} < g,$$
(2.4)

and

where the prime symbol (') indicates differentiation with respect to the dimensionless time variable  $\tau$ . Finally, the following spatial dimensionless variables are used:

$$u = \frac{\overline{x}}{y_0}$$
 and  $\delta = \frac{g}{y_0}$ . (2.5)

The dimensionless equations of motion can be written as

$$u''_{c}(\tau) + 2(\zeta + \zeta^{*}\rho^{*})u'_{c}(\tau) + (1 + \rho^{*2})u_{c}(\tau)$$

$$= \rho^{2} \sin(\rho\tau) + 2\zeta^{*}\rho^{*}\delta'(\tau) + \rho^{*2}\delta(\tau) \qquad \text{when } u \geq \delta,$$

$$u''_{o}(\tau) + 2\zeta u'_{o}(\tau) + u_{o}(\tau) = \rho^{2} \sin(\rho\tau) \qquad \text{when } u < \delta.$$
(2.6)

and

Note that the non-dimensionalization allows pre-computation of all the responses for all base displacement levels since the response has been scaled by  $y_0$ . This enables offline pre-computation of all information needed in the control method described in §4. Moreover, scaling the frequency

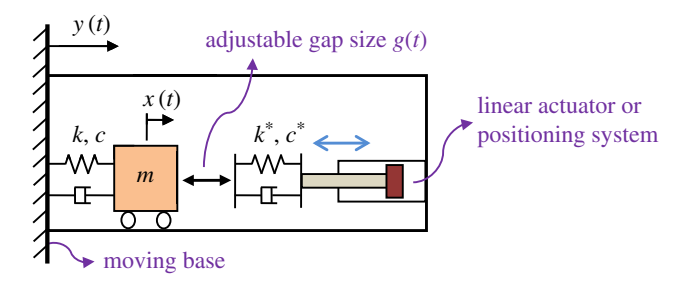


**Figure 1.** Mechanical model of the PWL harvester. The system is composed of a PWL oscillator with an adjustable gap size controlled by a linear actuator/positioning system. (Online version in colour.)

by  $\omega$  enables efficient selection of the parameters of the harvester system without the need for reconducting the analysis.

#### 3. Dynamic properties

The vibration behaviour of simple PWL oscillators has been studied extensively over the past few decades [43,44]. Nonlinear dynamic properties such as the well-known jump phenomenon have been observed in these systems. In order to efficiently analyse the steady-state dynamics of the proposed system for constant gap sizes, the previously developed BAA method is applied to find the solution to equation (2.6) by setting  $\delta'(\tau) = 0$ . First, the coordinates of the system in its closed and open state are analytically expressed as combinations of the linear transient response and the linear steady-state response

$$u_{c}(\tau) = e^{-\overline{\zeta}\overline{\rho}\tau}a_{c}\sin\left(\sqrt{1-\overline{\zeta}^{2}}\overline{\rho}\tau + \phi_{c}\right) + \frac{(\rho/\overline{\rho})^{2}\sin(\rho\tau - \theta_{c} + \psi)}{\sqrt{[1-(\rho/\overline{\rho})^{2}]^{2} + (2\overline{\zeta}\rho/\overline{\rho})^{2}}} + \delta\left(\frac{\rho^{*2}}{1+\rho^{*2}}\right)$$
and
$$u_{o}(\tau) = e^{-\zeta\tau}a_{o}\sin\left(\sqrt{1-\zeta^{2}}\tau + \phi_{o}\right) + \frac{\rho^{2}\sin(\rho\tau - \theta_{o} + \psi)}{\sqrt{(1-\rho^{2})^{2} + (2\zeta\rho)^{2}}},$$
(3.1)

where  $\overline{\rho} = \sqrt{1 + \rho^{*2}}$ ,  $\overline{\zeta} = (\zeta + \zeta^* \rho^*)/\sqrt{1 + \rho^{*2}}$ ,  $\theta_c = \tan^{-1}(2\overline{\zeta}\rho\overline{\rho}/(\overline{\rho}^2 - \rho^2))$  and  $\theta_o = \tan^{-1}(2\zeta\rho/(1 - \rho^2))$ ;  $[a_c, a_o]$  and  $[\phi_c, \phi_o]$  are scalar coefficients and phase angles of the linear transient responses, respectively. The angle  $\psi$  reflects the phase difference between the excitation and the linear steady-state responses.

The key idea of the BAA method is that an entire vibration cycle of the PWL oscillator can be obtained by coupling the responses in the closed and open states. The motion of one steady-state vibration cycle is schematically shown in figure 2. The BAA method assumes that a single vibration cycle has only one time interval when the response is in the closed state and only one time interval when the response is in the open state. These time intervals are denoted using  $T_c$  and  $T_o$ , respectively. Note that  $T = T_c + T_o$  is the period of the harmonic excitation. Next, a nonlinear optimization solver is used to solve for the unknowns  $a_c$ ,  $a_o$ ,  $\phi_c$ ,  $\phi_o$  and  $\psi$  in equation (3.1) by minimizing the residual of a set of compatibility conditions listed as follows:

$$u_{c}(0) = \delta,$$

$$u_{c}(T_{c}) = \delta,$$

$$u_{o}(T_{c}) = \delta,$$

$$u_{o}(T_{c} + T_{o}) = \delta,$$

$$u'_{c}(T_{c}) = u'_{o}(T_{c})$$

$$u'_{c}(0) = u'_{o}(T_{c} + T_{o}).$$

$$(3.2)$$

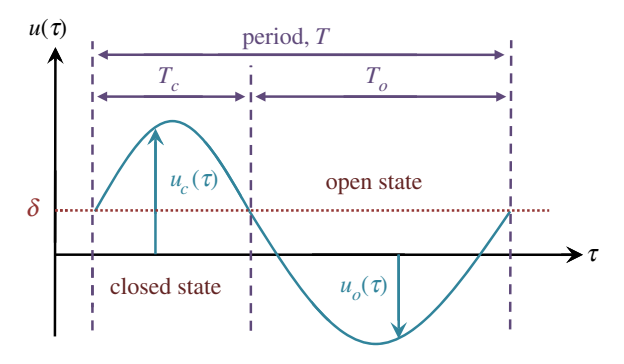


**Figure 2.** One steady-state nonlinear vibration cycle of the PWL oscillator for a constant gap size  $\delta$ . (Online version in colour.)

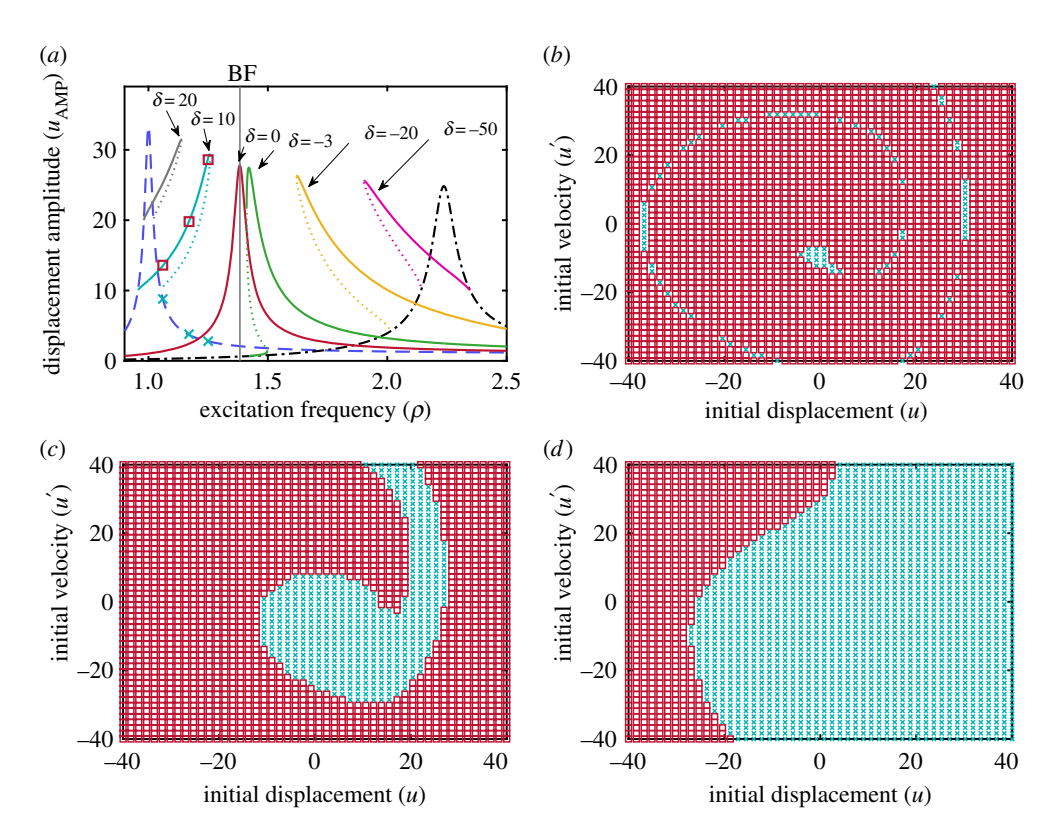


**Figure 3.** (a) Forced responses of the PWL oscillator for different gap sizes. (--) represents the linear response of the system in its open state; (-) represents the linear response of the system in its closed state; (-) and ( $\cdot\cdot\cdot$ ) represent the stable and unstable nonlinear responses when intermittent contact happens, respectively. (b-d) Basins of attraction for [ $\delta=10$ ,  $\rho=1.06$ ], [ $\delta=10$ ,  $\rho=1.17$ ] and [ $\delta=10$ ,  $\rho=1.25$ ], respectively. ( $\square$ ) represents the initial condition that converges to the nonlinear response and ( $\times$ ) represents the initial condition that converges to the linear response. (Online version in colour.)

The first four equations in equation (3.2) represent the displacement compatibility conditions at the transition moment when the dimensionless displacement u equals the dimensionless gap size  $\delta$  when the system switches from one state to the other. The last two equations in equation (3.2) represent the velocity compatibility conditions whereby the velocity of the mass must be continuous at the moment of transition. Note that  $T_c$  in equation (3.2) is also an unknown since the time fraction that the system stays in two linear states cannot be predetermined. The function 'Isqnonlin' in Matlab [45] was used in this work to solve for all the unknown parameters.

One nonlinear vibration cycle can then be constructed once these unknowns are solved. The detailed description of the BAA method can be found in [40].

The nonlinear forced responses of the PWL oscillator for different gap sizes  $\delta$  are computed using the BAA method and plotted in figure 3a. The system parameters used in this work are  $\zeta = 0.015$ ,  $\zeta^* = 0.015$  and  $\rho^* = 2$ . The linear response of the system when the gap is always closed and the linear response of the system when the gap is always open are also plotted in the figure. Figure 3a shows that the resonant frequency of the system can be shifted by changing the gap size  $\delta$ . The resonant frequency associated with  $\delta = 0$  is referred to as the bilinear frequency [43]. This resonant frequency can be lowered by increasing  $\delta$  and can be raised by decreasing  $\delta$ . This implies that the resonant frequency of the harvester can be tuned to match an arbitrary excitation frequency over the frequency range bounded by the natural frequencies of the linear systems by adjusting the gap to the appropriate size. Furthermore, nonlinear characteristics such as multistability, instability and jump phenomenon can be observed when  $\delta \neq 0$ .

Next, time integration is used to investigate the basins of attraction for the system since multiple stable periodic responses can be observed. The Runge–Kutta method [46] and the event function in Matlab [45] were used to conduct time integration. The results of  $\rho=1.06, 1.17$  and 1.25 when  $\delta=10$  are plotted in figure 3b-d. These figures show that the system, when  $\delta>0$ , can settle into either the nonlinear response where the intermittent contact happens or the linear response where there is no contact. Similarly, the system can settle into either the nonlinear response or the linear response where the gap is always closed when  $\delta<0$ . Furthermore, it is observed that the area of the basins of attraction of the nonlinear response shrinks significantly when  $\rho$  approaches the resonant frequency. Although the nonlinearity can provide a larger vibration motion when the excitation frequency is extremely close to the resonant frequency, it is also more likely that the system will jump from the nonlinear response to the linear response when it is slightly perturbed.

# 4. Methodology

A control method that combines BAA, signal measurement, and a gap adjustment mechanism for optimizing the vibration performance of the proposed PWL harvester is introduced in this section. In order to determine the gap size that can tune the system to resonance, the BAA method is employed to conduct two consecutive sweep processes. In the first sweep, the BAA method is used to sweep through the frequency range bounded by the natural frequencies of the linear systems (i.e. open and sliding systems) by setting  $\delta = 0$ . In this  $\rho$ -sweep process, the nonlinear solver is provided with random initial values at the starting frequency point. The solution that results in the minimum residual and that obeys the physical constraints is chosen for the frequency sweep [40]. Next, the peak response and the corresponding gap size at each frequency  $\rho$  is found by sweeping through the gap size  $\delta$ . The  $\delta$ -sweep process starts from  $\delta = 0$ using the  $\rho$ -sweep result as the initial value and ends at a  $\delta$  value where the solution can not be found using BAA. The results of the  $\delta$ -sweep process for five different  $\rho$  values are shown in figure 4a. The peak responses are indicated using ( $\bigcirc$ )'s in the figure. Note that when  $\rho$  is greater than the BF  $\delta$  is decreased to locate the peak response; while when  $\rho$  is less than the BF  $\delta$  is increased to find the peak response. The gap size associated with the peak response is referred to as the resonant gap size  $\delta_r$  in this paper. These resonant gap sizes are indicated using  $(\downarrow)$ 's in figure 4a.  $\delta_r$  represents the gap size that can theoretically provide the maximum steady-state vibration amplitude at a specified excitation frequency  $\rho$  if the excitation signal is perfectly harmonic. Figure 4a also shows that the vibration displacement amplitude is roughly proportional to  $\delta$ . By successively applying the  $\delta$ -sweep process to each excitation frequency  $\rho$ , the maximum response and the corresponding  $\delta_r$  over the bounded frequency range can be efficiently determined using the BAA method. The maximum response envelope and the corresponding  $\delta_r$ values over the frequency range are plotted in figure 4b.

With  $\delta_r$  values computed, the vibration amplitude of the PWL oscillator can be amplified by adjusting the gap size to approach  $\delta_r$  at any excitation frequency within the bounded frequency range. However, energy harvesters are rarely driven by perfectly a harmonic excitation with

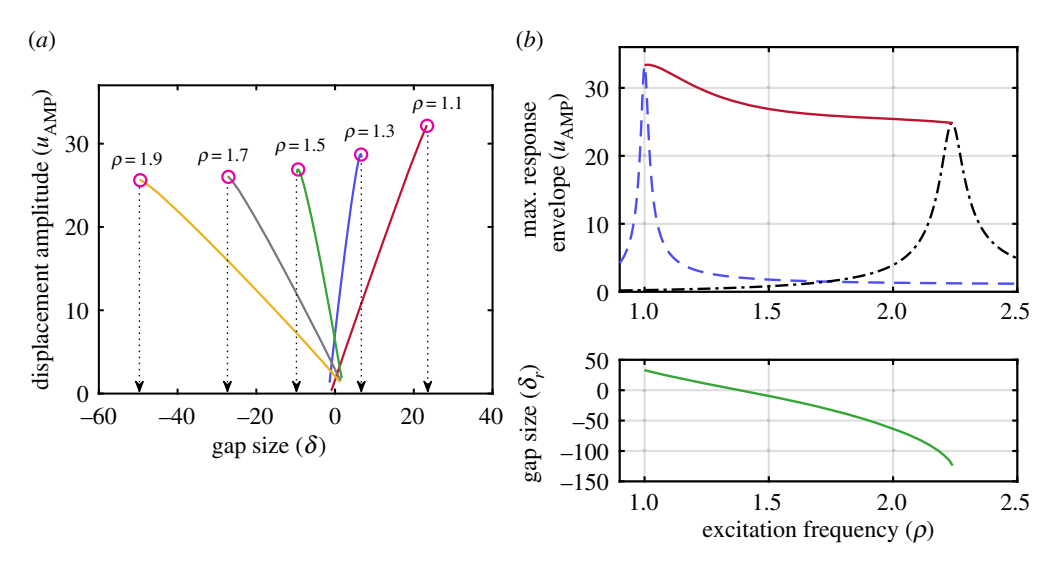


**Figure 4.** (a)  $\delta$ -sweep process. ( $\bigcirc$ )'s represent the peak responses and ( $\downarrow$ )'s represent the associated resonant gap sizes. (b) Maximum response envelope and resonant gap size over the bounded frequency range. (Online version in colour.)

a stable frequency and amplitude. Thus, a signal measurement and analysis process and a gap size adjustment strategy are introduced in this work. This control process assumes that the excitation signal is measurable through sensing devices and the gap size can be adjusted instantaneously based on the measured signal. Moreover, the excitation is assumed to contain a single frequency component that dominates the base motion at any given time. However, the excitation is accompanied by perturbation, and the dominant frequency and the corresponding amplitude can drift through time. If multiple significant frequencies are present in the spectrum, the one with the highest vibration amplitude should be chosen as the dominant frequency. The control process is described as follows:

- (i) The measured excitation signal is collected over a specified time duration  $T_s$ .
- (ii) The collected signal is analysed using frequency and amplitude estimators to extract the frequency  $\alpha_{\text{est}}$  and amplitude  $y_{0,\text{est}}$  that dominate the base motion.
- (iii) The  $\delta_r$  associated with  $\rho_{\rm est} = \alpha_{\rm est}/\omega$  that has been pre-computed using BAA is identified. Note that  $\rho_{\rm est}$  generally does not hit a frequency point that has been pre-computed.  $\delta_r$  at arbitrary  $\rho_{\rm est}$  can be obtained by interpolating adjacent  $\delta_r$  values.
- (iv) The optimized gap size  $\delta_{\rm opt}$  is determined by using only a fraction of  $\delta_r$  to avoid jumping from the nonlinear response to the linear response:  $\delta_{\rm opt} = a\delta_r$ , where 0 < a < 1.
- (v) The gap size is adjusted to  $g_{\text{opt}} = y_{0,\text{est}} \delta_{\text{opt}}$ .
- (vi) Steps (i)–(v) are repeated for next time window.

In this work, the dominant frequency and the associated amplitude are estimated using methods developed by Zhivomirov *et al.* [47] and Lyons [48], respectively. These methods build on discrete Fourier transform techniques, and estimate the frequency and amplitude by analysing the windowed signal in the frequency domain. Also note that the system is more likely to jump to the linear response if *a* is close to 1. The overall control process is summarized in figure 5.

Note that the computation of the optimized gap size  $g_{\rm opt}$  consists of two steps: (1) calculation of the non-dimensional gap size  $\delta_{\rm opt}$  for specific frequency points; and (2) identification of the dominant frequency  $\rho_{\rm est}$  and amplitude  $y_{0,\rm est}$ . The most computationally expensive part for determining  $g_{\rm opt}$  is step (1); however, this can be calculated in the design phase over the frequency range of interest in an offline pre-computation (i.e. the BAA method). Thus, there will not be a significant delay due to the control algorithm since the estimation of the frequency and

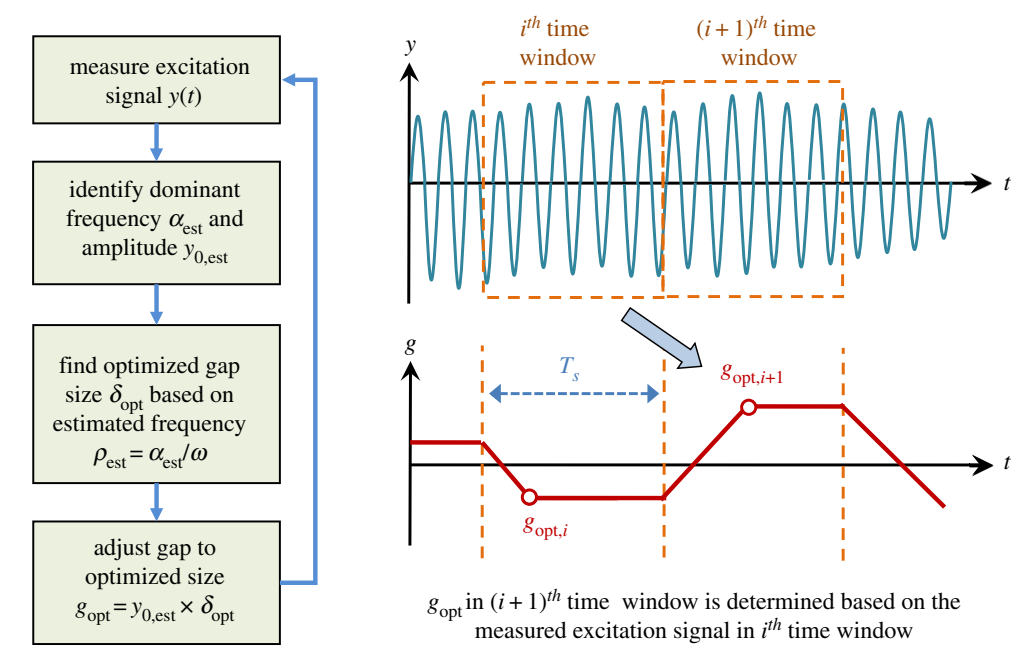


**Figure 5.** The control process that instantaneously optimizes the vibration performance of the PWL oscillator. (Online version in colour.)

amplitude will be done in a computationally efficient manner. Note that the control algorithm already includes a ramp rate for the change in the gap size for time-varying excitations so that the response will not drop to the lower responding linear response during the change in gap size. Therefore, any hardware limitations in changing the gap size would be included when optimizing the controller and setting the ramp rates for a specific application.

## 5. Numerical study

In this section, the PWL harvester integrated with the proposed control method is numerically investigated using time integration. Different excitation conditions are applied in case studies to validate the vibration performance of the system. The time duration used in the numerical studies is  $T_s = 40\tau$ , which is roughly equal to 6.4 times  $1/\omega$ . Note that the selection of  $T_s$  should cover at least a couple of vibration cycles so that the frequency and amplitude estimators can provide good estimates.

# (a) Unperturbed stationary excitation

The system subjected to a perfectly harmonic excitation with fixed excitation frequency and amplitude is studied first. In order to present the vibration amplitude variation, equations of motion with physical spatial variables, i.e. equation (2.4), are used for time integration. The actual excitation amplitude and frequency used in this case study are  $y_0 = 1$  and  $\rho = 1.15$ . Moreover, 94% of the resonant gap size is used as the optimized size to avoid the jump phenomenon, i.e. a = 0.94. Two gap size control strategies are compared in the study: (1) fixing the gap at the optimized size and (2) starting from g = 0 and gradually approaching the optimized gap size with the proposed control method. The mass is assumed to have zero initial displacement and zero initial velocity, i.e.  $(\bar{x}_0, \bar{x}_0') = (0,0)$ , in the simulation. The results are plotted in figure 6. Figure 6 shows that the signal estimators provide very accurate estimations for both the excitation frequency and amplitude when the base motion is perfectly harmonic. Furthermore, the vibration

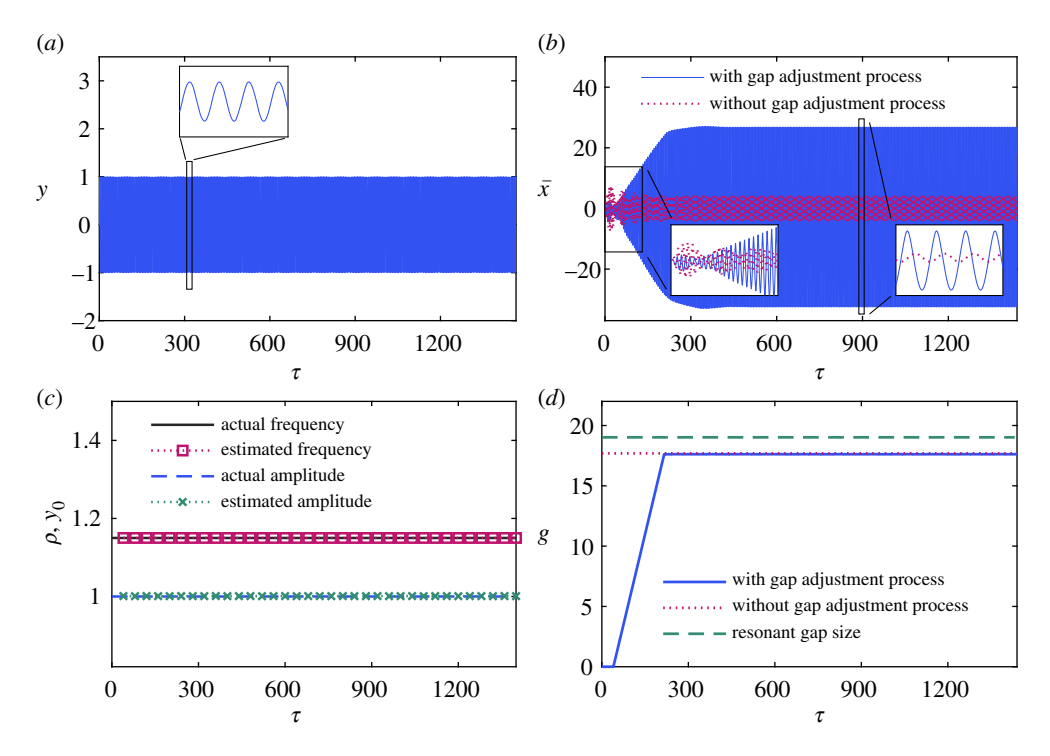


**Figure 6.** Numerical simulation with unperturbed stationary excitation. (*a*) Base excitation displacement. (*b*) Mass displacement. (*c*) Actual frequency and amplitude generated for excitation input and estimated values using the signal estimators. (*d*) Gap size history. (Online version in colour.)

response with the gradual adjustment strategy has a root mean square (RMS) amplitude of 19.81; however, the RMS amplitude of the vibration response without this adjustment strategy is only 2.92 even when the gap size is optimized. The vibration amplitude is increased by 6.78 times by employing the gradual adjustment strategy. When the gap size is fixed at the optimized size, the PWL oscillator converges to the linear response with a lower vibration amplitude since  $(\bar{x}_0, \bar{x}'_0) = (0,0)$  in this case is in the basin of the attractor of the linear response as discussed in §3. Thus, current PWL harvesters do not always provide an improved vibration performance in an arbitrary excitation frequency given a random initial condition since they do not have the gap adjustment mechanism. This new vibration energy harvester is able to accumulate vibration energy when the gap size is initially zero and gradually adjust the gap to the optimized size. This gradual adjustment process ensures that the system preserves the intermittent contact behaviour during the transient response. The controllable gap is required even when the system is subjected to stationary excitation.

### (b) Perturbed stationary excitation

The system subjected to a perturbed harmonic excitation with a fixed excitation frequency is studied in this case. In this study, the excitation is assumed to be perturbed by a normally distributed noise:  $y(\tau) = y_0 \sin(\rho \tau) + p(\tau)$ , where  $y_0 = 1$ ,  $\rho = 1.15$  and  $p(\tau)$  is the random perturbation with the variance being 35% of  $y_0$ . The results are plotted in figure 7. Figure 7 shows that the estimated frequency and amplitude both fluctuate around the  $\rho$  and  $y_0$  values used in the excitation input, respectively. In particular, the estimated amplitude has a larger variation due to the excitation perturbation. Furthermore, the system responses of using two optimized gap sizes are compared in figure 7b. The optimal gap size fluctuates due to changing estimated amplitude value as can be seen in figure 7c,d. When the system is tracking 88% of the resonant

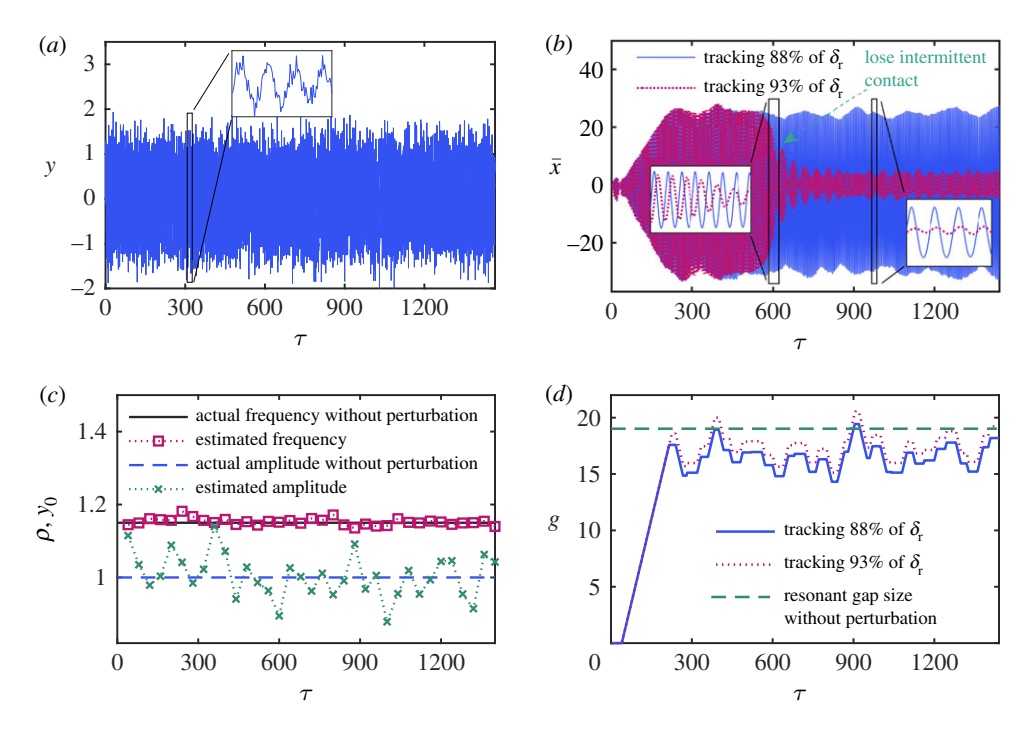


**Figure 7.** Numerical simulation with perturbed stationary excitation. (*a*) Base excitation displacement. (*b*) Mass displacement. (*c*) Actual frequency and amplitude generated for excitation input and estimated values using the signal estimators. (*d*) Gap size history. (Online version in colour.)

gap size, the PWL oscillator maintains intermittent contact over the entire simulation time range. By contrast, the system loses the intermittent contact when it is tracking 93% of the resonant gap size. This implies that the absolute optimized gap size needs to be reduced to prevent the system from jumping to the linear response due to the large variation in the excitation. The jump phenomenon significantly reduces the vibration performance. Thus, there is a trade-off between maintaining a high vibration amplitude and avoiding the undesired jump phenomenon. To determine the optimized *a* value, numerical studies can be used if there is knowledge about the expected excitation conditions. Furthermore, a control strategy that can bring the system back to the nonlinear response after the jump occurs is discussed in §5d.

#### (c) Drifting excitation

The case when the system is subjected to a gradually drifting excitation is studied next. In order to test how the proposed control method responds to changing excitation, both excitation frequency and amplitude are set up to drift through time. In this case study, the frequency gradually changes from  $\rho=1.05$  to  $\rho=2.2$  and the amplitude changes from  $y_0=2.0$  to  $y_0=0.5$  over the simulation time range. Note that a 35% perturbation of the amplitude is applied to the excitation signal and 87% of the resonant gap size is used for gap optimization. The results are shown in figure 8. Figure 8 shows that both the estimated frequency and amplitude fluctuate around the actual values due to the perturbation and signal drifting; however, the estimators track the trend of changing excitation very well. The response of using the adjustable gap with the proposed control method is compared with the response of using g=0 and g=20 in figure g=0 in figure g=0 and g=0 in figure g=0 in figure

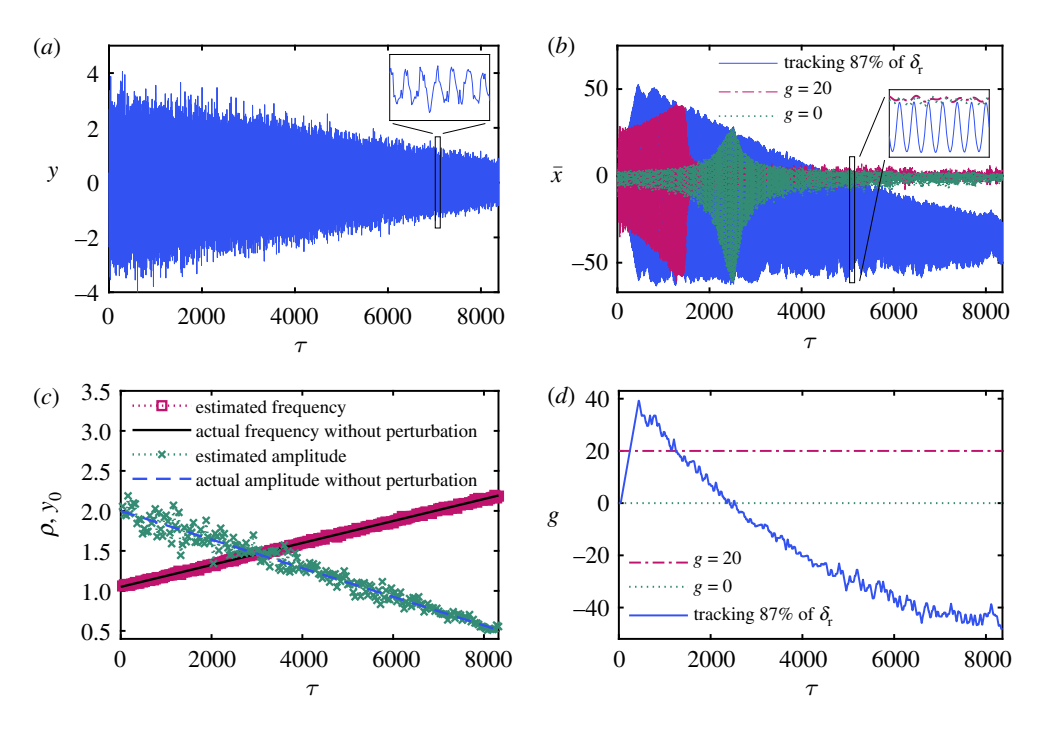


**Figure 8.** Numerical simulation with drifting excitation. (*a*) Base excitation displacement. (*b*) Mass displacement. (*c*) Actual frequency and amplitude generated for excitation input and estimated values using the signal estimators. (*d*) Gap size history. (Online version in colour.)

size is fixed at g = 20 and g = 0. Furthermore, it is observed that when g = 20 the system has a wider bandwidth than g = 0; however, the system quickly jumps to the linear response shortly after the excitation frequency passes the resonant frequency. The RMS vibration amplitudes are 32.94, 9.07 and 7.01 when using the adjustable gap, g = 20, and g = 0, respectively. In summary, the proposed control strategy provides the optimized vibration performance when the PWL harvester is driven by a changing excitation and the frequency drifts within the bounded frequency range.

#### (d) Excitation with abrupt changes

It has been shown that the proposed system can handle excitation with gradual changes in its frequency and amplitude. The case where the system is subjected to abruptly changing excitation is discussed next. In this case study, the system is subjected to piecewise stationary excitation with 35% perturbations in amplitude. The excitation frequency and amplitude within the three stationary regions are  $(\rho, y_0) = (1.05, 1.3)$ , (1.20, 2.0) and (1.70, 1.1), respectively. The excitation condition changes abruptly when it switches from one stationary region to the next. The result of applying the controllable gap is plotted in figure 9. Note that 87% of the resonant gap size is used for the optimized gap size. Figure 9b shows that the system loses the intermittent contact and tends to converges to the linear response shortly after the sudden changes in the excitation. In order to maximize the response, the gap size is adjusted to g = 0 to trigger the intermittent contact behaviour. Note that, as is shown in figure 3, the bistable regime does not exist when g = 0, and the nonlinear response is guaranteed for any motion because the mass will initiate and lose contact with the spring during a vibration cycle. Thus readjusting the gap size to g = 0 can always trigger the nonlinear response. Once the intermittent contact event occurs, the gradual adjustment process is activated to bring the system back to the optimized gap size to enhance the vibration performance. Note that this control strategy can also be applied in the circumstance

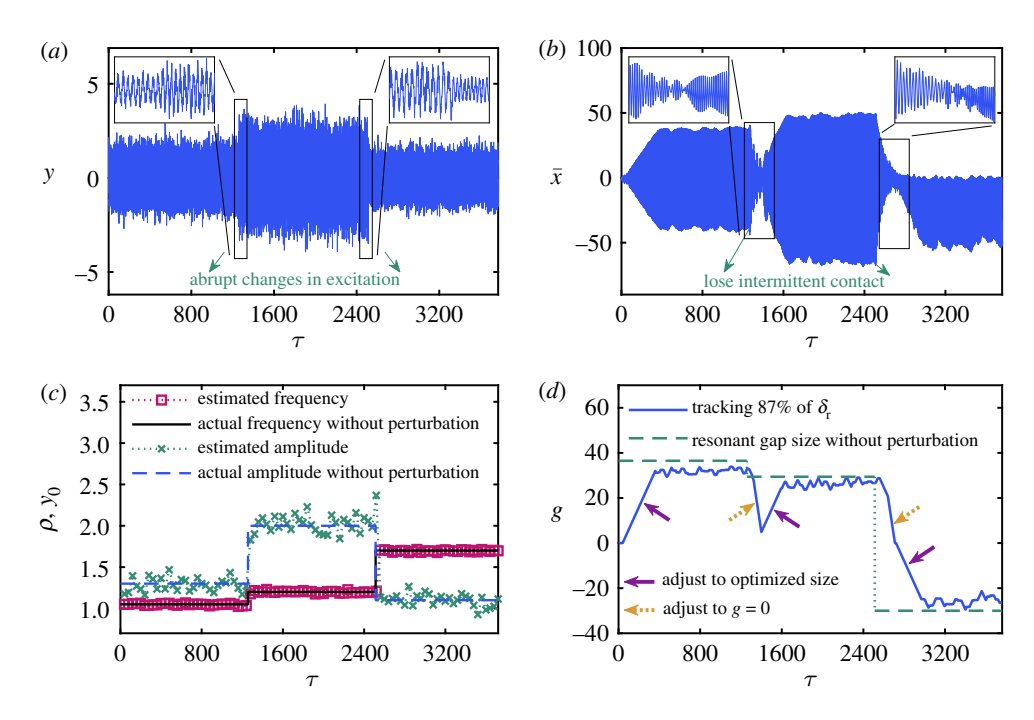


**Figure 9.** Numerical simulation with abruptly changing excitation. (*a*) Base excitation displacement. (*b*) Mass displacement. (*c*) Actual frequency and amplitude generated for excitation input and estimated values using the signal estimators. (*d*) Gap size history. (Online version in colour.)

where the system loses the intermittent contact due to perturbations in the excitation as discussed in §5b.

## 6. Energy generation discussion

In this section, the integration of the proposed mechanical model and electrical transducer is discussed. Note that either electromagnetic or piezoelectric transducers can be integrated with the proposed mechanical model to convert the kinetic energy into electrical energy; however, only the electromagnetic transducer is discussed in this work. Figure 10 shows the integrated vibration energy harvester consisting of the proposed mechanical oscillator and an electromagnetic transducer with  $R_H$  representing the electrical resistance of the harvester and  $f_e$  representing the electromotive force induced by the electromagnetic transducer. The equation of motion of the integrated system can be expressed as

$$\begin{cases}
\overline{x}_{c}''(\tau) + 2(\zeta + \zeta^{*}\rho^{*})\overline{x}_{c}'(\tau) + (1 + \rho^{*2})\overline{x}_{c}(\tau) + f_{e}(\tau) \\
= y''(\tau) + 2\zeta^{*}\rho^{*}g'(\tau) + \rho^{*2}g(\tau) & \text{when } \overline{x} \ge g \\
f_{e}(\tau) = \frac{\omega k_{t}k_{e}\overline{x}_{c}'(\tau)}{mR_{H}}
\end{cases}$$

$$\begin{cases}
\overline{x}_{o}''(\tau) + 2\zeta\overline{x}_{o}'(\tau) + \overline{x}_{o}(\tau) + f_{e}(\tau) = y''(\tau) \\
f_{e}(\tau) = \frac{\omega k_{t}k_{e}\overline{x}_{o}'(\tau)}{mR_{H}}
\end{cases}$$
(6.1)

where  $k_t$  is the motor constant and  $k_e$  is the electromotive force coefficient. Note that the electromotive force  $f_e$  can be thought of as a viscous damping force [49,50] and the equivalent electrical damping can be defined as  $c_e = \omega k_t k_e / mR_H$ . The instantaneous power absorbed by the

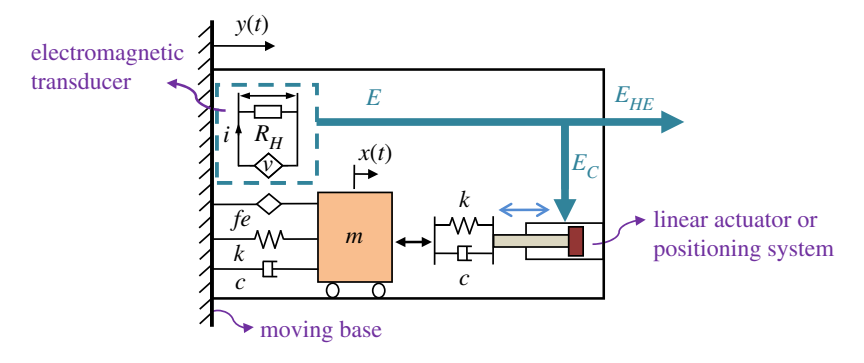


**Figure 10.** The integrated system consisting of the mechanical model and an electrical transducer. E represents the energy generated by the electromagnetic transducer;  $E_C$  represents the energy consumed by the controller;  $E_{HE} = E - E_C$  represents the harvested energy. Note that  $E_{HE} = \eta E$ , where  $\eta$  is the energy generation efficiency. (Online version in colour.)

electromagnetic transducer is  $P_{\text{inst}} = c_e(\overline{x}')^2$  and the energy generated by the electromagnetic transducer over a specific time range T is

$$E = c_e \int_0^T (\overline{x}')^2 d\tau. \tag{6.2}$$

Note that the linear positioning system will require a certain amount of energy to change its position. Therefore, the increase in harvested energy due to the proposed method must at least overcome the energy consumed by the actuator. This yields the following criterion:

$$\eta E_{wc} - E_{w/oc} > 0, \tag{6.3}$$

where  $E_{wc}$  is the energy generated by the transducer with the proposed control method,  $E_{w/oc}$  is the energy generated by the transducer without the proposed control method, and  $\eta \in [0, 1]$  is the energy generation efficiency that depends on the energy generated by the harvester relative to the energy consumed by the actuator. Note that  $\eta = 1$  represents the case where the actuator consumes no energy. Equation (6.3) can also be written as

$$\eta \int_{0}^{T} (\overline{x}'_{wc})^{2} d\tau - \int_{0}^{T} (\overline{x}'_{w/oc})^{2} d\tau > 0, \tag{6.4}$$

where  $\vec{x}'_{wc}$  is the velocity response of the system with the proposed control method and  $\vec{x}'_{wo/c}$  is the velocity response of the system without the proposed control method. The proposed controller can provide positive contribution to the energy harvesting only when equation (6.4) is satisfied. Thus, applications where this control method (that requires linear actuation) is used, and the actuator efficiency needed for specific applications requires further studies [51]. Furthermore, the system response is influenced by several parameters including the mechanical stiffness, mechanical damping and electrical damping.

#### 7. Conclusion

In this paper, an energy harvesting system with a PWL nonlinear oscillator and an adjustable gap is proposed. In this system, the resonant frequency of the device can be tuned to match the excitation frequency using a real-time control mechanism by adjusting the gap to the appropriate size. The proposed control method integrates the fast prediction of the optimized gap size, signal estimators, and a gap adjustment mechanism to optimize the vibration performance over a broad frequency range while also being able to achieve the best performance at resonance.

The nonlinear dynamic properties of the PWL oscillator are also discussed. The vibration performance of the proposed harvester with the proposed control method is numerically investigated in this work. The simulation results show that the proposed control method can enhance the vibration amplitude of the PWL harvester for both stationary and changing excitation conditions. The proposed system can achieve a better vibration performance than traditional PWL harvesters with the gap size fixed at a constant. Furthermore, the proposed energy harvesting strategy can be applied to piezoelectric or electromagnetic devices.

Data accessibility. Data for the numerical studies conducted in this work are available in the electronic supplementary material.

Authors' contributions. M.-H.T. and K.D. conceived the idea and methodology. M.-H.T. performed analyses, simulations, and drafted the paper. K.D. edited and finalized the paper.

Competing interests. We declare we have no competing interests.

Funding. This paper is based on work partially supported by the National Science Foundation under grant no. 1902408, program manager Dr Robert Landers. Any opinions, findings, and conclusions or recommendations expressed in this paper are those of the authors and do not necessarily reflect the views of the National Science Foundation.

Acknowledgements. M.-H.T. has been supported by the Future Academic Scholars Training program fellowship of the Department of Mechanical and Aerospace Engineering at The Ohio State University and the Presidential Fellowship from The Ohio State University Graduate School while working on this project.

#### References

- 1. Paradiso JA, Starner T. 2005 Energy scavenging for mobile and wireless electronics. *IEEE Pervasive Comput.* **4**, 18–27. (doi:10.1109/MPRV.2005.9)
- 2. Daqaq MF, Masana R, Erturk A, Dane Quinn D. 2014 On the role of nonlinearities in vibratory energy harvesting: a critical review and discussion. *Appl. Mech. Rev.* **66**, 040801 (23 pages). (doi:10.1115/1.4026278)
- 3. Ilyas A, Kashif SAR, Saqib MA, Asad MM. 2014 Wave electrical energy systems: implementation, challenges and environmental issues. *Renew. Sustain. Energy Rev.* 40, 260–268. (doi:10.1016/j.rser.2014.07.085)
- 4. Aderinto T, Li H. 2018 Ocean wave energy converters: status and challenges. *Energies* 11, 1250. (doi:10.3390/en11051250)
- 5. Wei C, Jing X. 2017 A comprehensive review on vibration energy harvesting: modelling and realization. *Renew. Sustain. Energy Rev.* **74**, 1–18. (doi:10.1016/j.rser.2017.01.073)
- Roundy S, Wright PK, Rabaey J. 2003 A study of low level vibrations as a power source for wireless sensor nodes. Comput. Commun. 26, 1131–1144. (doi:10.1016/S0140-3664(02)00248-7)
- 7. Jeon YB, Sood R, Jeong J-h, Kim S-G. 2005 MEMS power generator with transverse mode thin film PZT. Sens. Actuators A, Phys. 122, 16–22. SSSAMW 04. (doi:10.1016/j.sna.2004.12.032)
- 8. Renzi E. 2016 Hydroelectromechanical modelling of a piezoelectric wave energy converter. *Proc. R. Soc. A* **472**, 20160715. (doi:10.1098/rspa.2016.0715)
- 9. Williams C, Yates R. 1996 Analysis of a micro-electric generator for microsystems. *Sens. Actuators A, Phys.* **52**, 8–11. (doi:10.1016/0924-4247(96)80118-X)
- 10. Glynne-Jones P, Tudor M, Beeby S, White N. 2004 An electromagnetic, vibration-powered generator for intelligent sensor systems. *Sens. Actuators A, Phys.* **110**, 344–349. (doi:10.1016/j.sna.2003.09.045)
- 11. Arnold DP. 2007 Review of microscale magnetic power generation. *IEEE Trans. Magn.* 43, 3940–3951. (doi:10.1109/TMAG.2007.906150)
- 12. Mitcheson P, Miao P, Stark B, Yeatman E, Holmes A, Green T. 2004 MEMS electrostatic micropower generator for low frequency operation. *Sens. Actuators A, Phys.* **115**, 523–529. (doi:10.1016/j.sna.2004.04.026)
- Meninger S, Mur-Miranda JO, Amirtharajah R, Chandrakasan A, Lang JH. 2001 Vibration-toelectric energy conversion. *IEEE Trans. Very Large Scale Integr. VLSI Syst.* 9, 64–76. (doi:10.1109/ 92.920820)
- 14. Poulin G, Sarraute E, Costa F. 2004 Generation of electrical energy for portable devices: comparative study of an electromagnetic and a piezoelectric system. *Sens. Actuators A, Phys.* **116**, 461–471. (doi:10.1016/j.sna.2004.05.013)

- DuToit NE, Wardle BL, Kim SG. 2005 Design considerations for MEMS-scale piezoelectric mechanical vibration energy harvesters. *Integr. Ferroelectr.* 71, 121–160. (doi:10.1080/ 10584580590964574)
- 16. DuToit NE, Wardle BL. 2007 Experimental verification of models for microfabricated piezoelectric vibration energy harvesters. *AIAA J.* 45, 1126–1137. (doi:10.2514/1.25047)
- 17. Erturk A, Inman DJ. 2008 A distributed parameter electromechanical model for cantilevered piezoelectric energy harvesters. *J. Vib. Acoust.* **130**, 041002-1–041002-15. (doi:10.1115/1.2890402)
- 18. McInnes C, Gorman D, Cartmell M. 2008 Enhanced vibrational energy harvesting using nonlinear stochastic resonance. *J. Sound Vib.* **318**, 655–662. (doi:10.1016/j.jsv.2008.07.017)
- 19. Mann B, Sims N. 2009 Energy harvesting from the nonlinear oscillations of magnetic levitation. *J. Sound Vib.* **319**, 515–530. (doi:10.1016/j.jsv.2008.06.011)
- 20. Quinn DD, Triplett AL, Bergman LA, Vakakis AF. 2010 Comparing linear and essentially nonlinear vibration-based energy harvesting. *J. Vib. Acoust.* **133**, 011001-1–011001-8. (doi:10.1115/1.4002782)
- 21. Ramlan R, Brennan MJ, Mace BR, Kovacic I. 2010 Potential benefits of a non-linear stiffness in an energy harvesting device. *Nonlinear Dyn.* **59**, 545–558. (doi:10.1007/s11071-009-9561-5)
- 22. Blarigan LV, Danzl P, Moehlis J. 2012 A broadband vibrational energy harvester. *Appl. Phys. Lett.* **100**, 253904. (doi:10.1063/1.4729875)
- 23. Harne RL, Wang KW. 2013 Prospects for nonlinear energy harvesting systems designed near the elastic stability limit when driven by colored noise. *J. Vib. Acoust.* **136**, 021009-1–021009-8. (doi:10.1115/1.4026212)
- 24. Tehrani MG, Elliott SJ. 2014 Extending the dynamic range of an energy harvester using nonlinear damping. *J. Sound Vib.* **333**, 623–629. (doi:10.1016/j.jsv.2013.09.035)
- Cao J, Zhou S, Inman DJ, Lin J. 2015 Nonlinear dynamic characteristics of variable inclination magnetically coupled piezoelectric energy harvesters. J. Vib. Acoust. 137, 021015-1–021015-9. (doi:10.1115/1.4029076)
- 26. Luongo A, Zulli D. 2015 Nonlinear energy sink to control elastic strings: the internal resonance case. *Nonlinear Dyn.* **81**, 425–435. (doi:10.1007/s11071-015-2002-8)
- 27. Vijayan K, Friswell M, Khodaparast HH, Adhikari S. 2015 Non-linear energy harvesting from coupled impacting beams. *Int. J. Mech. Sci.* **96-97**, 101–109. (doi:10.1016/j.ijmecsci.2015. 03.001)
- 28. Liu JQ, Fang HB, Xu ZY, Mao XH, Shen XC, Chen D, Liao H, Cai BC. 2008 A MEMS-based piezoelectric power generator array for vibration energy harvesting. *Microelectron. J.* **39**, 802–806. (doi:10.1016/j.mejo.2007.12.017)
- 29. Marinkovic B, Koser H. 2012 Demonstration of wide bandwidth energy harvesting from vibrations. *Smart Mater. Struct.* **21**, 065006. (doi:10.1088/0964-1726/21/6/065006)
- 30. Xie L, Cai M. 2015 Increased energy harvesting and reduced accelerative load for backpacks via frequency tuning. *Mech. Syst. Signal Process.* **58-59**, 399–415. (doi:10.1016/j.ymssp.2015.01.012)
- 31. Soliman MSM, Abdel-Rahman EM, El-Saadany EF, Mansour RR. 2008 A wideband vibration-based energy harvester. *J. Micromech. Microeng.* **18**, 115021. (doi:10.1088/0960-1317/18/11/115021)
- 32. Soliman MSM, Abdel-Rahman EM, El-Saadany EF, Mansour RR. 2009 A design procedure for wideband micropower generators. *J. Microelectromech. Syst.* **18**, 1288–1299. (doi:10.1109/JMEMS.2009.2031695)
- 33. Hoffmann D, Folkmer B, Manoli Y. 2009 Fabrication, characterization and modelling of electrostatic micro-generators. *J. Micromech. Microeng.* **19**, 094001. (doi:10.1088/0960-1317/19/9/094001)
- 34. Julin Blystad L, Halvorsen E. 2010 A piezoelectric energy harvester with a mechanical end stop on one side. In 2010 Symp. on Design Test Integration and Packaging of MEMS/MOEMS (DTIP), Seville, Spain, 5–7 May, pp. 259–262. Piscataway, NJ: IEEE.
- 35. Le CP, Halvorsen E, Søråsen O, Yeatman EM. 2012 Microscale electrostatic energy harvester using internal impacts. *J. Intell. Mater. Syst. Struct.* 23, 1409–1421. (doi:10.1177/1045389X12436739)
- 36. Liu H, Lee C, Kobayashi T, Tay CJ, Quan C. 2012 Investigation of a MEMS piezoelectric energy harvester system with a frequency-widened-bandwidth mechanism introduced by mechanical stoppers. *Smart Mater. Struct.* 21, 035005. (doi:10.1088/0964-1726/21/3/035005)

- 37. Wu Y, Badel A, Formosa F, Liu W, Agbossou A. 2014 Nonlinear vibration energy harvesting device integrating mechanical stoppers used as synchronous mechanical switches. *J. Intell. Mater. Syst. Struct.* **25**, 1658–1663. (doi:10.1177/1045389X14533437)
- 38. Liu S, Cheng Q, Zhao D, Feng L. 2016 Theoretical modeling and analysis of two-degree-of-freedom piezoelectric energy harvester with stopper. *Sens. Actuators A, Phys.* **245**, 97–105. (doi:10.1016/j.sna.2016.04.060)
- 39. Dechant E, Fedulov F, Chashin DV, Fetisov LY, Fetisov YK, Shamonin M. 2017 Low-frequency, broadband vibration energy harvester using coupled oscillators and frequency up-conversion by mechanical stoppers. *Smart Mater. Struct.* **26**, 065021. (doi:10.1088/1361-665X/aa6e92)
- 40. Tien MH, D'Souza K. 2017 A generalized bilinear amplitude and frequency approximation for piecewise-linear nonlinear systems with gaps or prestress. *Nonlinear Dyn.* 88, 2403–2416. (doi:10.1007/s11071-017-3385-5)
- 41. Tien MH, Hu T, D'Souza K. 2018 Generalized bilinear amplitude approximation and *X-X<sub>T</sub>* for modeling cyclically symmetric structures with cracks. *J. Vib. Acoust.* **140**, 041012-1–041012-10. (doi:10.1115/1.4039296)
- 42. Tien MH, Hu T, D'Souza K. 2019 Statistical analysis of the nonlinear response of bladed disks with mistuning and cracks. *AIAA J.* 57, 4966–4977. (doi:10.2514/1.J058190)
- 43. Shaw SW, Holmes PJ. 1983 A periodically forced piecewise linear oscillator. *J. Sound Vib.* **90**, 129–155. (doi:10.1016/0022-460X(83)90407-8)
- 44. Natsiavas S. 1990 On the dynamics of oscillators with bi-linear damping and stiffness. *Int. J. Non-Linear Mech.* **25**, 535–554. (doi:10.1016/0020-7462(90)90017-4)
- 45. MATLAB. 2018 version 9.5 (R2018b). Natick, MA: The MathWorks Inc.
- 46. Shampine LF, Reichelt MW. 1997 The MATLAB ODE suite. SIAM J. Sci. Comput. 18, 1–22. (doi:10.1137/S1064827594276424)
- 47. Zhivomirov H, Nedelchev I, Vasilev R. 2016 A method for single-tone frequency estimation. *Rom. J. Acoust. Vib.* **13**, 20–24.
- 48. Lyons R. 2012 *Reducing FFT scalloping loss errors without multiplication*, pp. 215–225. New York, NY: John Wiley & Sons, Ltd.
- 49. Tang X, Zuo L. 2009 Towards meso and macro scale energy harvesting of vibration. Volume 10: Mechanical systems and control, parts A and B. ASME Int. Mechanical Engineering Congress and Exposition.
- 50. Tai WC, Zuo L. 2017 On optimization of energy harvesting from base-excited vibration. *J. Sound Vib.* 411, 47–59. (doi:10.1016/j.jsv.2017.08.032)
- 51. Genest R, Bonnefoy F, Clément AH, Babarit A. 2014 Effect of non-ideal power take-off on the energy absorption of a reactively controlled one degree of freedom wave energy converter. *Appl. Ocean Res.* 48, 236–243. (doi:10.1016/j.apor.2014.09.001)